This is a repository copy of *Deformation at Krafla and Bjarnarflag geothermal areas, Northern Volcanic Zone of Iceland, 1993-2015*.

White Rose Research Online URL for this paper:
http://eprints.whiterose.ac.uk/118745/

Version: Accepted Version

Article:

Accepted Manuscript

Deformation at Krafla and Bjarnarflag geothermal areas, Northern Volcanic Zone of Iceland, 1993-2015

Vincent Drouin[a,*], Freysteinn Sigmundsson[a], Sandra Verhagen[b], Benedikt G. Ófeigsson[c], Karsten Spaans[d], Sigrún Hreinsdóttir[e]

[a]*Institute of Earth Sciences, University of Iceland, 101 Reykjavík, Iceland*
[b]*Delft University of Technology, department of Geoscience and Remote Sensing, 2628 CN Delft, Netherlands*
[c]*Icelandic Meteorological Office, 101 Reykjavík, Iceland*
[d]*COMET, School of Earth and Environment, University of Leeds, Leeds, United Kingdom*
[e]*GNS Science, Lower Hutt 5040, New Zealand*

Abstract

The Krafla volcanic system has geothermal areas within the Krafla caldera and at Bjarnarflag in the Krafla fissure swarm, 9-km south of the Krafla caldera. Arrays of boreholes extract geothermal fluids for power plants in both areas. We collected and analyzed InSAR, GPS, and leveling data spanning 1993-2015 in order to investigate crustal deformation in these areas. The volcanic zone hosting the geothermal areas is also subject to large scale regional deformation processes, including plate spreading and deflation of the Krafla volcanic system. These deformation processes have to be taken into account in order to isolate the geothermal deformation signal. Plate spreading produces the largest horizontal displacements, but the regional deformation pattern also suggests readjustment of the Krafla system at depth after the 1975-1984 Krafla rifting episode. Observed deformation can be fit by an inflation source at about 20 km depth north of Krafla and a deflation source at similar depth directly below the Krafla caldera. Deflation signal along the fissure swarm can be reproduced by a 1-km wide sill at 4 km depth closing by 2-4 cm per year. These sources are considered to approximate the combined effects of vertical deformation associated with plate spreading and post-rifting response. Local deformation at the geothermal areas is well resolved in addition to these signals. InSAR shows that deformation at Bjarnarflag is elongated along the direction of the Krafla fissure swarm ($\sim$4 km by $\sim$2 km) while it is circular at Krafla ($\sim$5 km diameter). Rates of deflation at Krafla and Bjarnarflag geothermal areas have been relatively steady. Average volume decrease of about 6.6×10^5 m^3/yr for Krafla and 3.9×10^5 m^3/yr for Bjanarflag are found at sources

---

*Corresponding author
Email addresses:* vjp1@hi.is (Vincent Drouin), fs@hi.is (Freysteinn Sigmundsson)

located at $\sim$1.5 km depth, when interpreted by a spherical point source of pressure. This volume change represents about 8×10^{-3} m^3/ton of the mass of geothermal fluid extracted per year, indicating important renewal of the geothermal reservoir by water flow.

1. Introduction

The installed capacity to generate electricity in geothermal power plants in Iceland is 665 MW, or about 24% of total electricity generated (Statistics Iceland, 2016). Extraction of geothermal fluids can generate subsidence in the surroundings of power plants as conditions in geothermal reservoirs are modified. Here we study the ground deformation at two geothermal areas within the Krafla volcanic system, NE Iceland, where two power plants are operated.

There is a growing interest in geothermal energy due to its renewability (Axelsson et al., 2015). The rechargeability of a geothermal reservoir depends on the influx of ground water from surrounding areas and the influx of heat to the reservoir. In a fully sustainable production scenario the volume of geothermal fluid extracted by the power plant is in balance with the influx of water and heat. If the volume of geothermal fluid extracted exceeds the rechargeability of the geothermal reservoir, the reservoir may become depleted. Lack of complete recharge of geothermal reservoirs during utilization can results in ground subsidence. Subsidence 'bowls' may form around arrays of utilized boreholes (e.g., Hole et al., 2007; Keiding et al., 2010) and can extend along faults (e.g., Ali et al., 2016). In extreme cases in sedimentary settings, the cumulative subsidence can exceed 10 m after long periods of utilization (Bromley et al., 2013). Deformation caused by geothermal exploitation is often attributed to pore-pressure change and/or thermal processes within the geothermal reservoirs (Chen, 2011; Vasco et al., 2013; Im et al., 2017).

The Krafla volcanic system (Fig. 1) is one of the main volcanic systems in the Northern Volcanic Zone (NVZ) of Iceland (Sæmundsson, 1974; Hjartardóttir et al., 2015). It has a central volcano with a 9 x 7 km caldera bordered by rhyolithic domes. Its fissure swarm, the surface expression of rifting with repeated dike intrusions, extends 40 km to the south and 50 km to north from the center of the caldera (Hjartardóttir et al., 2012). The Krafla volcanic system has two known extended periods of high eruptive activity during

the Holocene (Sæmundsson, 1991). The current period started around 2600–2800 years BP. Prior to it, the eruptive activity was concentrated in the Fremrinámar volcanic system, whose central volcano lies 35 km south of Krafla caldera.

Two rifting events are documented for the Krafla volcanic system in historical times (last 1100 years): the 1724–29 Mývatn Fires (Thoroddsen, 1907–1915) and the 1975-84 Krafla Fires (Einarsson, 1991; Buck et al., 2006). During the latter, at least 20 dikes were intruded, with nine resulting in fissure eruptions. Dikes were intruded 20 km to the south and 60 km to the north of a shallow magma chamber under the Krafla caldera. The pressure center of the chamber inferred from inflation/deflation patterns is near Mt. Leirhnjúkur in the center of the caldera. All the eruptive activity took place within and to the north of the caldera. The maximum cumulative opening due to diking was 8-9 m, north of the caldera (Tryggvason, 1984). Rifting and diking, and deformation after such events, has e.g. also been studied in Afar (Nooner et al., 2009; Hamling et al., 2014), Djibouti (Smittarello et al., 2016), and Hawaii (Lundgren et al., 2013). Post-rifting adjustment and associated deformation signals may occur over wide areas for decades after rifting events, influencing both horizontal and vertical displacements. Such regional adjustment has thus to be considered when addressing local deformation in areas influenced by rifting.

Gradual uplift of the Leirhnjúkur area continued until 1989, five years after the last eruption, due to pressure increase in the shallow magma chamber. The area then began to subside, at an average rate of ∼5 cm/yr from 1989 to 1992. The subsidence rate has decayed exponentially since, with the estimated subsidence rate lower than 3 mm/yr in 2006 (Sturkell et al., 2008). After 1995, the maximum rate of subsidence shifted from directly above the shallow magma chamber, towards the array of boreholes in the Leirbotnar area within the Krafla caldera (Fig. 1). Subsidence has also been observed around the array of boreholes at Bjarnarflag geothermal area (Sturkell et al., 2008).

There are a number of other large scale deformation signals influencing in the Krafla region, most importantly the plate spreading across the NVZ. According to the MORVEL2010 plate-motion model, the North-American plate and the Eurasian plate separate at the rate of about 18 mm/yr in a direction N104.5°E (DeMets et al., 2010). A similar rate is inferred from GPS observations (Drouin et al., 2017). Additionally, a broad uplift pattern has been detected north and north-east of Krafla. Candidate explanations include magma accumulation near the crust/mantle boundary (de Zeeuw-van Dalfsen et al., 2004; Metzger and Jónsson, 2014) and/or post-rifting relaxation (Ali et al., 2014). Inflation occurred in

3

2007-2008 in the Þeistareykir central volcano (20 km NW of Krafla) suggesting magma intrusion (Metzger et al., 2012). Glacial isostatic adjustment (GIA) caused by retreat of ice caps in Iceland since ∼1890 is also influencing the area (Árnadóttir et al., 2009; Auriac et al., 2014; Compton et al., 2015). However, the GIA contribution in the Krafla area is on the order of a few mm/yr in the vertical and less than 1 mm/yr in the horizontal (Drouin et al., 2017). In addition to these sources, deflation along the Krafla fissure swarm has been identified from geodetic observations (Sigmundsson et al., 1997; Metzger and Jónsson, 2014).

There are two main geothermal fields in the Krafla volcanic system: one near the center of the Krafla caldera, another 9 km south, at Námafjall (Fig. 1). Landsvirkjun, the national power company of Iceland, operates a geothermal power plant in both geothermal fields. The main one, located in the Krafla caldera, began its operation in 1977 with an initial production of 30 MW. Most of the boreholes used by the Krafla power plant are located in the Leirbotnar area within the caldera (Fig. 1), later referred to as the Krafla geothermal area. In 1996 a second turbine was installed, with the power plant reaching its nominal capacity of 60 MW in 1997. Its main purpose is to provide electricity for towns in northeast Iceland. The other power plant is located at Bjarnarflag, on the west flank of the Námafjall volcanic ridge. Its operation began in 1969 and has an installed capacity limited at 3 MW. It is mainly used to provide hot water to the town of Reykjahlíð and a nearby geothermal pool. Both power plants have been continuously operating since they entered production, even during the 1975-1984 Krafla rifting episode.

Water and steam extraction rate has been fairly stable at the Bjarnarflag power plant since 1977, with an average of 1500-2500 kT (kilotons) per year (Fig. 2). At the Krafla power plant, water extraction rate doubled after 1995 to supply the second turbine. Since 2000, on average 9000 kT of water and steam have been extracted per year. Re-injection of water started in 1999, and the rate of injection has been increasing with time. In 2014, it was more than 4000 kT per year.

2. Geodetic data

In 1938, a triangulation network was set up across the NVZ centered at Krafla volcano to test Wegener's continental drift hypothesis (Niemczyk, 1943; Tryggvason, 1984). The 100 km long network was re-measured in 1965, using electronic distance measurements (EDM) and triangulation, and repeated every few years for the next two decades

4

together with observations along leveling profiles (Gerke, 1974; Wendt et al., 1985). During the Krafla rifting episode 1975-84, terrestrial geodesy techniques (leveling, theodolite and electronic distance measurements, tiltmeters) were extensively used for measuring the ground deformation (Tryggvason, 1984). New space geodesy techniques were introduced early in the region: Global Positioning System (GPS) geodesy in the late 1980's (Foulger et al., 1992; Heki et al., 1993) and interferometric analysis of synthetic aperture radar images (InSAR) from satellites in the early 1990's (Sigmundsson et al., 1997). Since the 1990's, GPS and InSAR measurements have been favored over the historical terrestrial geodetic techniques. The geodetic dataset for the period 1993-2015 consists mostly of repeated GPS measurements and SAR acquisitions, as well as some leveling surveys. With the exception of continuous GPS stations that log data all year around, measurements reported here were acquired during the summer months, from the end of June to mid-September. Geodetic observations acquired at the same time of the year mitigate the influence of the seasonal deformation cycle in Iceland on time series analysis of the various datasets (Grapenthin et al., 2006; Drouin et al., 2016). In the following, data time intervals refer to intervals from summer to summer (e.g., 1995-2000 should be interpreted as summer 1995 to summer 2000).

2.1. Leveling

Following the Krafla rifting episode 1975-84, leveling surveys were conducted to monitor the Krafla and Bjarnarflag geothermal areas in 1989, 1995, 2000, 2005 (Sturkell et al., 2008), and 2010 (Theodórsson and Búi, 2011). Measurements concentrate on six main leveling lines across the Bjarnarflag geothermal area and Krafla caldera, all linked together. Leveling benchmarks are spaced between 250 and 2000 meters from each other. Here we use the data from 1995, 2000, 2005, and 2010 provided by Landsvirkjun.

Average vertical velocities are obtained by differentiating the height measurements at each site between two surveys and dividing them by the time separation between the two measurements. Leveling velocities are relative by nature; one station in the network is used as a reference. Under the condition that the difference between the geoid and the ellipsoid is uniform over the area of interest, GPS vertical velocities known at some of the stations can be used to reference the entire network to a global frame. The 1995 to 2005 and 2005 to 2010 velocities inferred from leveling are shown in Figs. 3 and 4, respectively. Local subsidence of about 5-7 mm/yr is observed at both Krafla and Bjarnarflag geothermal areas

5

when compared to their surroundings.

2.2. *GPS*

The first Iceland country-wide GPS survey was conducted in 1986 and included a few sites near Krafla (Foulger et al., 1993). Large-scale GPS surveys of the NVZ began in 1987 for monitoring tectonic displacements and other deformation processes (Jahn et al., 1990). Additional surveys were conducted in the NVZ in 1990 and 1992 to study post-rifting relaxation after the Krafla rifting episode (Foulger et al., 1992; Heki et al., 1993; Hofton and Foulger, 1996). From 1992, surveys were conducted in the area every few years until 2002. Since then, the area has been measured on a yearly basis, although only with sparse observations until 2012. An extensive gravimetry survey was conducted by ISOR, the Icelandic Geosurvey in 2012. The University of Iceland carried out the precise GPS geodetic measurements at the gravity sites. In the following years, dense GPS measurements were acquired by University of Iceland in collaboration with the Delft University of Technology, Netherlands.

Within the Krafla caldera, the GPS sites HVIT, RAHO, and VITI have been measured the most regularly for the longest time (see Fig. 1 for location). The oldest and closest site to the Bjarnarflag geothermal area is NAMA, located on Mt. Námafjall. It has been measured sporadically since 1986. The near-surroundings of the Bjarnarflag power plant only started to be monitored with GPS in detail in summer 2012, but have been measured every summer since.

The first continuous GPS station in the Krafla region, MYVA, was installed in 2006 in the village of Reykjahlíð, SW of Krafla. It is operated by the Bavarian Academy of Sciences and Humanities (Germany) in collaboration with Landmælingar Íslands (National Land Survey of Iceland). Two additional continuous GPS stations were installed by the University of Iceland in collaboration with the Landsvirkjun power company in 2011 and 2012: KRAC (next to Krafla power plant) and BJAC (south of the Bjarnarflag area).

GPS data from over 80 GPS sites in the Krafla area have been analyzed at University of Iceland using GAMIT/GLOBK 10.6. Sites positions were evaluated in the ITRF2008 reference frame using over 100 worldwide reference stations in a similar manner as described by Drouin et al. (2017). The resulting time series cover the time period from summer 2002 to summer 2015. The time series were then analyzed with the Tsview software (Herring and McClusky, 2009) to derive velocities with realistic uncertainties at each GPS

6

site. Using this approach, we derived three-dimensional displacement velocities at each site measured at least twice during the chosen time intervals. Velocities are referenced to the stable Eurasian plate and show a clear westward motion of about 10 mm/yr as well as subsidence for all sites in the Krafla volcanic system (see Figs. 5 and 6).

2.3. InSAR

The Northern Volcanic Zone of Iceland is well suited for InSAR measurements as vegetation there is sparse or non-existent. However, the area is usually covered with snow from fall to late spring. Thus only images acquired in July, August, and September have good enough coherence to be used for interferometric analysis.

SAR images began to be acquired over North Iceland in 1992 by the ERS-1 satellite mission. Images over the Krafla volcanic system were first used by Sigmundsson et al. (1997) to observe magma chamber deflation and post-rifting deformation processes. Since then many SAR satellite missions have acquired data over the area. Here we have use images from ERS, Envisat (Envi), TerraSAR-X (TSX), and Radarsat-2 (RS2) missions. Most of the images were granted by the Committee on Earth Observation Satellites (CEOS) through the Icelandic Volcanoes Supersite project, following the nomination of Iceland as a Permanent Geohazard Supersite in 2013 (FUTUREVOLC, 2016).

InSAR measures one-dimensional ground displacement in the line-of-sight (LOS) of the satellite, *i.e.* along the ground-satellite direction. Satellite tracks are categorized in ascending tracks (satellite approaching the North Pole region, following approximately a south-north direction) or descending tracks (satellite approaching the South Pole region, following approximately a north-south direction). SAR instruments on board satellites can be right-looking (images acquired on the right of the satellite direction) or left-looking (images are acquired on the left of the satellite direction). All tracks analyzed here are right-looking. Five tracks are descending (ERS T9, T52, T281; Envisat T230; TerraSAR-X T49) and four ascending (Envisat T281; TerraSAR-X T56, T147; Radarsat-2). In addition to the track and look direction, the look angle (angle from the vertical) at which the images are acquired will determine the LOS. All satellites have almost north-south tracks in Iceland, which makes InSAR fairly insensitive to deformation in the north direction. A satellite acquiring images with a small look angle will be mostly sensitive to the vertical motion while acquisitions with a large look angle will sense more the horizontal E-W motion. It is beneficial to have both ascending and descending tracks covering the

7

same area, as the contribution of displacements along the east-west direction to the LOS displacements will be reversed.

Data from each InSAR track were processed with the StaMPS software using the permanent scatters (PS) and small baseline combined processing (Hooper, 2008). With the exception of TSX track T49 and T56, all tracks were cropped to our area of interest to keep the processing time reasonable. Topographic effects were corrected using a digital elevation model (DEM) provided by DLR, the German Space Agency. This DEM is a preliminary product from the TanDEM-X mission and has a spatial resolution of 12 m and a vertical precision of less than 10 m.

For each time series, we obtained images of the LOS displacements for the satellite acquisitions included in the processing. An average LOS velocity field was also derived for each time series.

2.4. Time intervals

In order to make best use of our data and investigate possible temporal variation in the deformation field, we divided our dataset into six time intervals: 1993-1995, 1995-2000, 2000-2003, 2004-2010, 2009-2014, and 2012-2015. These time intervals were mainly chosen according to the time spanned by the various InSAR satellites (see Fig. 2). Table 1 gives an overview of the data for each of the time intervals.

Figures 3 to 6 give an overview of the observed ground deformation and the geothermal fluid utilization for each time interval. Note that Figure 3 presents 1993-2003 data and therefore covers the 1993-1995, 1995-2000, and 2000-2003 time intervals combined. Profiles across the InSAR velocity fields reveal a 5-km wide subsidence signal in Krafla and 2-km wide subsidence signal in Bjarnarflag when compared to the area in between (Figs. 3 to 6). The InSAR velocity fields also show that the local deformation pattern appears to be circular at Krafla while it is elongated along the fissure swarm at Bjarnarflag.

The 1995-2000 and 2009-2014 time intervals have the best InSAR time series: over 10 images, which are fairly well distributed over long time periods. Other time intervals have less than 10 images per time series, which are poorly distributed over the time period (2004-2010) or spanning a short time interval (1993-1995, 2000-2003, 2012-2015). The 2012-2015 time interval has the most extensive GPS dataset. However, the 2009-2014 time interval covers a longer time and has thus longer time series, which gives more reliable velocities. Too few GPS measurements were conducted in the 2004-2010 time interval

8

to contribute significantly to the deformation observation dataset. Leveling observations cover only 1995 to 2010, therefore only the 1995-2000, 2000-2003, and 2004-2010 time intervals includes leveling data (average velocities between the two surveys covering better the period). Leveling surveys were conducted in a similar way, we thus expect the data over each of these time intervals to be of equal quality. Overall the 1995-2000 and 2009-2014 time intervals have better deformation datasets than the other time intervals.

The division of our data set into time periods takes into consideration the limitations of the data. There are methods that can provide a higher temporal resolution than the one considered here (e.g., Pritchard and Simons, 2006; Grandin et al., 2010), but these require in general more extensive data sets. Our data (InSAR, GPS, and leveling) have been collected each year in the summer time, which means we can only realistically achieve a 1-year resolution at best. Second, the deformation rates are small (1-2 cm/yr) which make any year-to-year deformation measurements really sensible to noise in the data. Finally, apart from a decay in the subsidence rate in the 1990's, deformation rates appears to be relatively stable.

2.5. *Areas of high deformation gradient*

Average LOS velocity fields derived from InSAR time series provide a good coverage of the deforming areas. We search for areas of high deformation gradients by applying the following formula on each of the inferred LOS average velocity fields:

$$S = \sqrt{(\delta LOS/\delta E)^2 + (\delta LOS/\delta N)^2} \tag{1}$$

The gradient magnitude S is obtained by taking the derivative of the LOS velocity field along East and North directions using GMT routine *grdmath* (Wessel and Smith, 1998). To minimize noise and emphasize the fast deforming areas, all LOS velocity fields were also stacked together before calculating the gradient magnitude (Fig. 7). Gaps in the velocity fields were filled using Delaunay triangulation.

Steep topography feature are sources of error during InSAR processing because they cause layovers and shadows in the SAR images. Thus high gradient magnitude near steep topography may be an error rather than an indication of fast deforming area. On the other hand, high gradient magnitude on relatively flat areas can be considered good indicator of areas with high deformation gradients. Therefore, areas with slope over 0.2 (20 m relief over 100 m distance) along the East direction were masked out in Fig. 7.

9

We infer a few areas of reliable high deformation gradients: around Leirhnjúkur, north of the Krafla geothermal field, west of Hvíthólar, and west of Bjarnarflag geothermal field (Fig. 7). In Krafla, high InSAR gradients concentrate along the eruptive vents of the Krafla rifting episode but also east of them, across Leirbotnar. In Bjarnarflag, the high gradients area outlines an elongated high deformation area 600-800 meters west of the power plant. Although it follows the general direction given by the fissure swarm, no surface fault is directly associated with this high InSAR gradient area.

3. Model

In order to study the deformation due to local processes at Krafla and Bjarnarflag geothermal areas, there is need to isolate the deformation signal from the more regional deformation due to plate spreading and other long wavelength deformation processes.

3.1. Regional deformation in the Krafla volcanic system

The Krafla volcanic system is subject to large-scale deformation sources in addition to deformation related to the shallow Krafla magma chamber and local geothermal processes. The regional horizontal displacement field is dominated by spreading across the divergent plate boundary in North Iceland. The geothermal areas are located close to the present central axis of the plate spreading in the Northern Volcanic Zone (Drouin et al., 2017). It has been suggested that the observed regional deformation pattern reflects a combination of plate spreading and deep magma accumulation near the crust/mantle boundary (de Zeeuw-van Dalfsen et al., 2004; Metzger and Jónsson, 2014). An alternate model by Ali et al. (2014) suggests post-rifting relaxation signal instead of deep magma accumulation to explain the observations. These studies constrain their model using GPS velocities and/or InSAR time series only from a descending satellite track.

Here, we use TSX T49 descending track, TSX T56 ascending track, and GPS velocities, all spanning 2009-2014, to constrain the long wavelength deformation patterns. We compared this dataset to the model by Metzger and Jónsson (2014). It includes a backslip plate spreading model, centered on the Krafla fissure swarm, and a deep Mogi point pressure source (Mogi, 1958) north of Krafla. Although having a spreading segment axis aligned along the Krafla fissure swarm (as suggested by previous studies) provides a fairly good fit to our GPS data and descending InSAR data, it doesn't explain well the ascending InSAR data. Furthermore, using horizontal GPS velocities, Drouin et al. (2017) infer that

10

the plate spreading central axis doesn't appear to follow the direction given by the Krafla fissure swarm south of the caldera.

An elongated deflation signal along the fissure swarm is clearly observed in the InSAR time series. Here, we propose that this elongated signal reflects a combination of stretching of the plate boundary across a weak zone of the Krafla fissure swarm (structural weakness) and readjustment of the fissure swarm after the Krafla Fires, both by thermal processes as well as stress relaxation. The repeated dike intrusions during the 1975-1984 rifting episode may have opened fractures, thus allowing more water to enter deep into the fissure swarm, resulting in increased thermal cooling of the surrounding rocks. Stress relaxation following the Krafla rifting episode and plate spreading across a crustal weakness zone (recently activated fissure swarm) could also contribute to this subsidence signal along the Krafla fissure swam.

We implement an inversion process to put constraints on the sources causing these deformation processes (parameters are shown in Table 2). Secular plate spreading is modeled as by Drouin et al. (2017). Local deformation signals due to the Krafla magma chamber and the Krafla and Bjarnarflag geothermal sources are modeled as by Sturkell et al. (2008), considering three separate point sources of pressure, fixing their locations. We included a deep point source of pressure increase in the same location and depth as Metzger and Jónsson (2014) but searched for its best fitting volume change. Furthermore, we place a deep point source of pressure decrease under the Krafla caldera in the location suggested by Drouin et al. (2017) and search for its best fitting volume change. This two deep sources setup explains well the observed northward horizontal displacements in our study area and may indicate readjustments at depth following the Krafla rifting episode. The subsidence and contraction along the Krafla fissure swarm is modeled as a single horizontal contracting sill (Okada, 1992). The length and direction of the dislocation is inferred from the zone where dikes were intruded during the Krafla rifting episode (Tryggvason, 1984). Its depth, width, and closing rate are kept free. A contracting dike from the surface to a depth of a few kilometers in the same location was also considered. However, for a similar rate of subsidence, this model induces a much larger horizontal contraction signal which is not present in our observations. Therefore the contracting sill model was chosen. Figure 8 shows the location of the sources utilized in the inversion as well as the results of the inversion. InSAR velocity fields were resampled to a $0.01°$E by $0.005°$N grid prior to inversion to keep the computational time reasonable. We use a grid search approach to

11

find the best fitting parameters for the model by minimizing the chi-square. We allow for a constant offset for each InSAR LOS velocity field and the Up component GPS velocity field. InSAR LOS velocity fields have a relative reference and thus it is appropriate to consider an offset for them before estimating the fit to the model. Vertical GPS velocities are absolute, but in our model we didn't account for the GIA signal, which generates uplift of few mm/yr in the area (Drouin et al., 2017). Our area of interest spans a short latitude range (65.6° to 65.75°). Over this distance (~17 km) the vertical GIA signal varies by less than a mm and can be considered constant, as the closest edge of Vatnajökull (the main source of the GIA signal) is at about 90 km from Bjarnarflag. Therefore, GIA can be accounted for by considering an offset for the vertical GPS velocities in our modeling. Table 2 shows the results of the inversion. We found that the contracting sill is located at about 3.3 km depth, is 0.6 km wide, and closes at a rate of approximately 28 mm/yr for 2009-2014. On the surface, this model results in about 10 mm/yr subsidence along segment of the Krafla fissure swarm that was active in 1975-1984. The constant offset for GPS vertical velocities is estimated 4.9 mm/yr, similar to the uplift expected from the GIA in this area for the time period of our study (Drouin et al., 2017).

3.2. Geothermal areas

Here we focus on a smaller area to look for temporal variation of the deformation (Figs. 3 to 6). We use inversion to infer changes in both the regional deformation signal and the deformation processes in the geothermal areas for each time interval. For the regional deformation field, we looked for possible variations from our previous results over the Krafla volcanic system 2009-2014. We use the same model setup for the regional sources as described previously (Table 2) but keep free the closing rate of the sill, the volume change of the deep inflation, and the volume change of the deep deflation. The smaller area of interest allows us to remove the plate spreading segments *GOR3* and *HFF4* from the model, and to fix the locking depth of the plate spreading segments *Krafla* and *Fremrinamar* to 7 km, the approximate value for this area according to Drouin et al. (2017) Fig. 9. The InSAR velocity fields were resampled to keep the computational time reasonable and reduce the effects of correlation between the individual PS scatterers. Points within 2 km from Bjarnarflag (16.85°W, 65.64°N) and 4.5 km from Krafla (16.77°W, 65.70°N) were resampled to a 200 m grid while points outside were resampled to a 400 m grid. Thus more points are considered in the areas over the main geothermal deformation signal compared

to the areas outside them. This is a simple method of InSAR data resampling, comparable to the other resampling method such as the quadtree approach (Fukushima et al., 2005) that considers highest density of points in areas that show the largest deformation signal. Each resampled InSAR point has the average LOS velocity and location from all points included in the "pixel". The LOS standard deviation is computed for each resampled point and this is considered the uncertainty of that point. A minimum uncertainty of 0.1 mm/yr is fixed for points that have a still lower value resulting from this approach. The standard deviation is then used to weight each InSAR observation during the inversion process.

3.2.1. Simple model for geothermal sources

When modeling the local deformation signal at Krafla and Bjarnarflag, we initially used source coordinates from Sturkell et al. (2008). The model includes three deflating Mogi sources: at 1.5 km depth under Bjarnarflag geothermal area, at 1.5 km depth under Leirbotnar geothermal area, and at 2.5 km depth under Leirhnjúkur (approximate location of the pressure center of the shallow basaltic magma chamber under Krafla caldera). We first used a grid search approach to find the best fitting parameters for the regional deformation model (see previously) and the best fitting volume change for Leirhnjúkur, Leirbotnar, and Bjarnarflag pressure source. In the second step, we fixed the three shallow pressure sources and ran 1000 bootstrap inversions to determine a more accurate volume change for the deep sources, the closing rate of the sill, and their uncertainties. Then we fixed the regional deformation model and ran 1000 bootstrap inversions to determine more accurately the volume change of the shallow pressure sources and their uncertainties. For each bootstrap inversion, observations are resampled randomly within their 1-sigma uncertainties and simulated annealing is used to determine the best fitting volume changes. As previously, we allow for an offset for each InSAR velocity field and the leveling velocities. The vertical GPS velocities are corrected for the 4.9 mm/yr offset corresponding to the GIA uplift, the value found previously when inverting the regional deformation field.

Figures 9 and 10 and Table 3 give an overview of the results from this two step inversion. Results for three of the five sources ($Deep_{deflation}$, $Deep_{deflation}$, $Leirhnjukur$) are shown in Fig. 9 and the remaining two ($Leirbotnar$, $Bjarnarflag$) are shown in Fig. 10. Location of the sources is shown in Fig 8. Comparison between observations and best fitting models for each time interval are shown in Figs. S1 to S6 in Supplementary Material. The closing rate of the sill appears to diminish steadily with time from 1993 to 2015.

The strength of the deep inflation source also decays with time, and is insignificant in the last time interval. The strength of the deflation of the deep source below Krafla caldera also shows a general decline. For the geothermal deformation sources, we find an average volume change of -6.6x10^5 m^3/yr for $Krafla$ and -3.9x10^5 m^3/yr for $Bjarnarflag$ in the 1993-2015 period.

3.2.2. Deformation based on extraction and injection of geothermal fluids

The extraction/injection data and the known location of each borehole provides an opportunity to link the observed deformation with the volume of geothermal fluid extracted/injected at Krafla and Bjarnarflag. Instead of using a single Mogi source for each of the geothermal areas as above, here we used the extraction and injection rates at each of the boreholes to predict the deformation field. In this model, we include an array of Mogi sources, with one Mogi source for each borehole utilized. To keep the model simple, we assume the extraction/injection of geothermal fluid happens at the similar level in the geothermal reservoir and thus choose to have the same depth for each of the Mogi sources. In this approach, there is a Mogi source at each location where boreholes intersect the given depth. A total of 35 Mogi point sources of pressure are considered, about 25 of them being concentrated in a 3 km by 2 km area in Leirbotnar. In this approach one can expect a violation of the assumption of a Mogi model, that each source should be located in an homogeneous half-space and not interact with other sources. Pascal et al. (2014) studied the interaction of such nearby pressure sources and found discrepancies to become significant for a source separation less than four times the radii of the sources (up to 20%). Therefore, this model approach can provide insights into the relation between geothermal utilization and observed deformation but the estimated values should be taken with care. We thus here only consider a model where the volume change (in m^3) of each source is set proportional to the mass (in tons) of water extracted/injected at the borehole it models. Such a model can test if the observed surface deformation can be related to the array of utilized boreholes in each of the fields.

We set up a grid search to find the depth and which proportion of the extracted/injected volume best explains the surface deformation. The regional model parameters are also inverted for during this search. Following trial and error, we considered a depth range from 500 m to 2500 m, in steps of 200 m, and a proportion of extracted/injected mass in the range from 0 to 30x10^{-3} m^3/ton in steps of 2x10^{-3} m^3/ton. The volume change

14

of the pressure source below Leirhnjúkur was kept free to account for possible changes in the magma chamber. We searched for the best depth and proportion for each period at Krafla only, Bjarnarflag only, and both Krafla and Bjarnarflag simultaneously. Results for Bjarnarflag only indicate a best depth a 2500 m (the search range upper boundary) for each time period and a variable best fitting proportion. Results for Krafla only are similar to results for both Krafla and Bjarnarflag simultaneously. For 1993-1995, 1995-2000, 2000-2003, the best depth is close to 1900-2100 m and the best proportion is 24-28x10^{-3} m^3/ton. For later time intervals (2004-2010, 2009-2014, 2012-2015), the best depth is about 700-1100 m and the best proportion about 4-6x10^{-3} m^3/ton. Grid search results show a clear trade-off between the depth and the proportion, the deeper the sources are the larger the proportion needs to be. Considering all the time intervals gives an overall minimum at a proportion of 6x10^{-3} m^3/ton and a depth of 900 m. When ignoring the 2012-2015 interval, which has somewhat poorer fit than the other intervals, we find an overall minimum at a proportion of 8x10^{-3} and a depth of 1100 m. We demonstrate results from this model for a depth of 1000 m for Mogi sources and a volume change equal to 8x10^{-3} m^3/ton of the extracted/injected mass of geothermal fluids (Figures S7 to S12 in Supplementary Material). The regional deformation parameters and the Leirhnjúkur volume change were inverted for using the same approach as in section 3.2.1. The predicted regional deformation (Fig. S13 in Supplementary Material) is very similar to the one predicted by the model with a single source at each geothermal area (Fig. 9) and the Leirhnjúkur source appears to deflate only during 1993-2003.

Pressure and temperature has been monitored in selected wells in the Krafla and Bjarnarflag areas that are not in utilization, revealing some changes over time but also variation from one well to another (e.g., Egilson et al., 2015). At Krafla, a long time series of observations in well KJ-10, not perturbed by direct utilization from any nearby well, indicates a systematic cooling at observation depth of 800 m depth by about 0.5°C/year since 1976. At this well the main signal in the pressure history is a drop of about 5 bar, mirroring an increase in production, with most of this change taking place 1995-1997 and smaller fluctuations thereafter. In Bjarnarflag, a time series of pressure and temperature change is available from 600 m depth in hole B-5, the deepest level of observation in that area. Pressure has remained relatively stable since 1987, with fluctuations less than 0.5 bar and no long term change. Temperature has also remained stable; since 2002 the cumulative temperature change has been less than one degree, with some irregular variations in an

15

earlier time interval from 1985-2002 on the order 5-10 degrees. It is, however, uncertain if these conditions at monitoring wells are representative of the deeper parts of the geothermal areas and the crustal volumes next to boreholes in utilization. In general, some mining of heat related to enhanced water flow can be expected in areas of geothermal utilization.

We explore the hypothesis that thermal contraction contributes to the observed deformation. Such approach has been taken by Ali et al. (2016) using a series of dislocation sources to explain deformation at the Brady Hot Springs geothermal field (Nevada). Here we consider thermal contraction taking place in spherical sources. For that purpose we seek a relation for equivalence between a Mogi source volume change and change due to thermal contraction of a spherical volume. We use equations 2a (first half) and 2c in Masterlark and Lu (2004), and the relation between internal pressure change in a Mogi source, ΔP, and its volume change ΔV_{Mogi} which equals $\Delta P \pi r^3 / G$, where r is the radius of the source and G the shear modulus. Combining these we find:

$$\Delta V_{Mogi} = \Delta T V_t \alpha_t \tag{2}$$

Temperature change of ΔT in a spherical volume V_t produces the same surface deformation field as Mogi source, with volume change given by the above relation were α_t is the linear coefficient of thermal expansion. Therefore $\Delta T V_t$, the volume of cooling times the temperature change in this model, can be directly derived from the previously found volume change of the source ΔV_{Mogi} by dividing it by α_t. Considering $\alpha_t = 1 \times 10^{-5}\,°\text{C}^{-1}$, the average volume change of -6.6x10^4 m^3/yr found when inverting for a single source at Krafla requires $\Delta T V_t$ = -6.6x10^9 m$^3 \cdot °$C/yr. If temperature change of the reservoir would be -0.5°C/yr, then a volume of 13.2x10^9 m^3 (a 1.5 km radius sphere) would be needed. This shows that minor cooling of a geothermal reservoir, difficult to detect at boreholes in utilization, could contribute to the deformation fields at Krafla and Bjarnarflag.

In the case of the model with a source at each of the boreholes, we found a proportion of 8x10^{-3} m^3/ton between the source volume (ΔV_{Mogi}) and the geothermal fluid mass extraction/injection (M_{gf}). Using equation (2), we find that $\Delta T V_t / M_{gf}$ = 800 m$^3 \cdot$ton$^{-1} \cdot °$C. Therefore, over a year, for a cooling of 0.5°C, the volume of cooling rock is approximately 1600 m^3/ton of the mass of extracted geothermal fluid. For geothermal extraction rate of 5x10^5 tons/yr like that of a "medium producing well" at Krafla, the resulting cooling volume would be 0.8x10^9 m^3 (a 576 m radius sphere). Energy balance (e.g. Ali et al., 2016) can be used to evaluate how much heating of water or boiling in the roots of the

16

geothermal system would be required for this heat mining to take place (see section 3 of Supplementary Material).

4. Discussion

The preceding analyses assume the observed deformation processes can be modeled with deformation sources embedded within a uniform elastic halfspace. For the geothermal areas, we decide to keep our models as simple as possible by only considering pressure point sources. Future studies with alternative approach, such as finite element modeling of a thermo-poro-elastic behaviour considering fluid flow (e.g., Rinaldi et al., 2010) may provide further insight. Despite simplicity, our models and observations confirm significant deformation due to geothermal processes both in the Krafla and Bjarnarflag areas. Within our study period, the deformation rate at Krafla was highest in the 1990's, but became relatively stable after around 2000 (InSAR time series in Fig. 3–6). This observation is also confirmed by inversion results (Figs. 9 and 10). In Bjarnarflag, observations (Figs. 3–6) indicate that the rate of deflation may have increased somewhat during the study period. This trend is also visible in the inversion results (Fig. 10).

The model with a single source at Krafla and Bjarnarflag and the model with a source at each borehole in utilization provide a similar fit to the data (Figs S1-S12 in Supplementary Material). Both model also find a reduction of the deformation rate of the non geothermal sources (Fig. 9 and Fig. S13 in Supplementary Material). There is large deflation signal associated with the shallow magma chamber during 1993-1995, in the model with a single source at Krafla and Bjarnarflag (Fig. 9C). It is then very small ($< 3x10^4$ m^3) for 1995-2003 before becoming insignificant in the later time intervals. In the model with the source at each borehole (Fig. S13C), the decay is not as abrupt and the deflation is more significant in 1995-2000 and 2000-2003 ($\sim$7-8x10^4 m^3). These results are in agreement with the exponential decay with time of the pressure variation in the shallow magma chamber beneath Leirhnjúkur inferred by Sturkell et al. (2008).

The main difference between the two models is that while the volume change of the source is kept free in the first model (Fig. 10), it is locked to the utilization of geothermal fluid in the second model (Fig. S14 in Supplementary Material). In the first model, the inferred volume changes are similar for both the Krafla and Bjarnarflag geothermal areas between 2004 and 2015 (Fig. 10). However, more than four times the amount of geothermal fluid was extracted at Krafla after 2004 compared to Bjarnarflag (Fig. 2). Re-injection

17

of geothermal fluid at borehole KJ-26 in Leirbotnar became significant after 2003 and may reduce the deflation rate Krafla of the Krafla geothermal area. However, only a third of the extracted fluid is being re-injected, and Krafla net extraction rate is still more than three times Bjarnarflag extraction rate. In addition, injection would reduce the deflation signal in the case this signal is cause by pressure decrease in the reservoir but not in the case the deflation is caused by thermal cooling, in which case the injection will induce additional cooling and deflation. This could also indicate a faster heat influx in the Krafla geothermal reservoir than in the Bjarnarflag geothermal reservoir. Another explanation could be that the deflation of the Bjarnarflag geothermal areas is increasing with time (Fig. 10) due to process other than geothermal fluid extraction. This apparent increase in deflation rate could suggest that the Bjarnarflag source is trying to account for the diminishing rate of deflation along the fissure swarm and is more sensitive to it than the Krafla source. A third explanation could relate to the fact that the shape of the deforming area is different at Krafla and Bjarnarflag, but a similar point pressure source model is used for both areas in the inversion process, and could therefore influence the volume inversion results.

In the model using information about geothermal fluid extraction/injection, we find a greater depth and higher proportion for the first time intervals (1993-1995, 1995-2000, 2000-2003) than for the following time intervals. One reason for that could be the lack of GPS data for the earlier time intervals that can put additional constrains to the later time intervals. Another reason could be that the model is trying to account for some deeper seated deformation signal between 1993 and 2003 which could be from volcanic or geothermal origin. In the latter case, this could be a response of the Krafla geothermal reservoir to the increase of geothermal fluid extraction by factor of two during the 1990's. For Bjarnarflag, this model has a maximum of subsidence below the array of boreholes while the observed maximum is located further to the west. In the case that the observed deformation is solely the effect of geothermal extraction in Bjarnarflag, this would imply a path for geothermal fluid to travel from beneath the high deformation area to the array of boreholes.

In our model based on information about extraction and injection of geothermal fluid, we explored the possibility that thermoelastic contraction of 0.5°C/yr near the boreholes is causing most of the observed deformation. To generate the same amount of deformation, poroelastic contraction over the same volume would require a change of 11 bar/yr (see section 4 of supplementary material). However, borehole logging (Egilson et al., 2015)

shows no indications of significant pressure loss in recent years at the boreholes measured. Therefore, if poroelastic contraction is the source of the deformation, the pressure drop in the geothermal reservoir would have to be very small (<0.1 bar/yr). This would then indicate that the geothermal reservoir is unrealistically large (about 1.2×10^{12} m^3, a 6.7 km radius sphere ; see section 4 of supplementary material). Therefore we suggest that thermoelastic contraction is the dominating source of deformation in our study area, similarly as suggested by Im et al. (2017) for geothermal utilisation in the long term, when pressure conditions in geothermal reservoirs remain relatively stable.

The elongated pattern of contraction and subsidence along of the Krafla fissure swarm could be caused by a combination of processes: i) thermal contraction along the Krafla fissure swarm (Sigmundsson et al., 1997), ii) post-rifting adjustment (Ali et al., 2014), and iii) local subsidence caused by plate spreading over a structural weakness in the crust (Pedersen et al., 2009; Islam et al., 2016). The simple analytical models presented here cannot differentiate between the possible contribution of each of these sources. This signal appears to slowly decay with time, consistent with expected behavior of post-rifting adjustment and also eventually from a thermal contraction signal.

For 2009-2014, the best fitting closing rate along the fissure swarm inferred from the regional deformation field ($\sim$28 mm/yr, Table 2) is smaller than the best fitting closing rate inferred from the local deformation field ($\sim$41 mm/yr, Table 3). The difference between these two values indicates that additional contraction along the fissure swarm may occur locally in the Krafla and Bjarnarflag areas. It can't be excluded that part of this additional contraction signal along the fissure swarm would be influenced by geothermal fluid extraction. Most of the fractures crossing the geothermal reservoir are expected to follow the direction of the fissure swarm, and the geothermal fluid extraction is supposed to occur along these fractures. Therefore part of the deflation signal might follow the fissure swarm. However, no model is presented here to explore this possibility. A numerical modeling approach would be required (e.g., finite element modeling) to allow a lower permeability along the fissure swarm than outside it.

Since 2004, we observe about 5-8 mm/yr of subsidence in Krafla for a net extraction rate of 6-9 Mtons/yr of geothermal fluid. This is about a 1 mm/yr of subsidence per Mtons/yr of net extraction, which is fairly similar to another geothermal power plant located in Hellisheiði (SW Iceland). There the current subsidence rate is about 20 mm/yr for an extraction rate of about 38 Mt/yr and injection rate of about 22 Mtons/yr (Budzińska,

19

2014; Juncu et al., 2017).

The approach we suggest here to define areas of high deformation gradients (Fig. 7) reveals that in addition to Leirhnjúkur, Leirbotnar, and the western boundary of Bjarnarflag, there is a high deformation area west of Hvíthólar. No boreholes have been extracting or injecting water in this area, and no activity was recorded there during the Krafla rifting episode but it was difficult to access. The gradient of deformation in this area appears to have decayed with time, making future ground studies less likely to provide information about the deformation process taking place. Existing InSAR data is thus probably the best source of information about this signal.

The models presented here provide a reasonably good fit to the observed deformation. However, a few points would need to be address in further studies of the area. InSAR residuals (Figs. S1 to S6 in Supplementary Material) show a similar pattern depending if the satellite track is ascending or descending. In ascending InSAR time series (Envi T230, TSX T56, TSX T147, and RS2), residuals show a NE-SW gradient. In ascending InSAR time series (ERS T9, T52, T281, Envi T281, TSX T49, there is a negative residuals area east of the central axis of the fissure swarm. These residuals indicate that some deformation processes are not properly accounted for in the current model. The deep inflation and the deep deflation below the Krafla volcanic system explain the observations reasonably well, especially in the North direction. However, this two sources model is likely to be a simplification of a more complex regional deformation processes. Post-rifting relaxation is expected to have generated observable deformation between 1993-2015 (Ali et al., 2014). The deep inflation and deflation model presented here could indicate magma migration at depth and/or pressure re-equilibrium of the magma system after the intrusions occurring between 1975-1984. A detailed numerical model of the 1975-1984 rifting episode and post-rifting signal, considering variable material properties, would be required to validate these hypotheses.

There is an increasing demand for geothermal energy in Iceland. A new power plant is under construction in Þeistareykir, 20 km NW of the Krafla caldera. It will have an initial production capacity of 90 MW, and is designed for up to 200 MW. GPS and InSAR have been acquired over the area for over 20 years, and plans are to monitor closely the ground deformation when the new power plant enters in production. The GPS network was densified in 2010 and a new continuous GPS station (THRC) was installed in the region in 2011.

20

Finite element modeling, taking into account the topography, the rheology, and the thermal structure in the Krafla area, as well as time-dependent processes, is warranted for further study of the various deformation processes taking place in the area. However, deformation measurements alone are not sufficient to constrain all the parameters of this model. Therefore, there is a need in further modeling to consider additional datasets providing complementary constrains e.g., seismic tomography, MT, gravimetry surveys, boreholes recordings, and petrology. Such model would be better suited to search for the processes responsible for the deflation signal along the fissure swarm and if any part of this signal could be caused by geothermal fluid extraction.

5. Conclusions

Leveling, GPS, and InSAR observations between 1993 and 2015 show that, in addition to the complex regional deformation, local surface displacements occur at two geothermal areas in the Krafla volcanic system. After discriminating between regional and geothermal processes, we infer that geothermal processes cause subsidence in both areas at an average rate 5 mm/yr. An elongated contraction and subsidence signal along the Krafla fissure swarm indicates eventual thermal contraction, readjustment following the Krafla rifting episode, and/or plate spreading over a weakness in the crust. Apart from the plate spreading, the regional deformation field decays with time and thus may reflect a post-rifting relaxation signal. There is no post-2003 evidence for significant pressure change in the magma chamber below Leirhnjúkur which was active during the Krafla rifting episode. A single Mogi source at each geothermal area appears to give similar results to a modeling approach using an array of Mogi sources (one source for each borehole). When using a model with a Mogi source at each borehole, the ratio between the source volume change and the mass of geothermal fluid extracted is about $8\mathrm{x}10^{-3}$ m^3/ton, and the inferred depth of extraction is about 1 km.

6. Acknowledgments

Figure 1: **A)** Footprint of SAR satellites tracks in the Northern Volcanic Zone of Iceland. Background shows glaciers (white), water bodies (blue) and shaded terrain (from green to brown for low to high). The elements of the Þeistareykir (Þ), Krafla (K), Fremrinámar (F), Askja (A), Kverfjöll (Kv), and Bárðarbunga (B) volcanic systems include central volcanoes (dashed lines) and their fissure swarms (transparent gray areas). **B)** Krafla and Bjarnarflag area. Leveling benchmark (yellow circles), GPS benchmarks (green triangles), continuous GPS sites (green triangles and white hexagons), and boreholes (blue hexagons). Background shows shaded topography, Krafla caldera (comb lines), 1975-84 lavas (dark gray area), and main road (black line). **C)** Krafla area. Boreholes which were used for production between 1993 and 2015 are shown with purple hexagons, and those which were not used during this period are shown with gray hexagons. Path of boreholes which are not vertical are shown with blue lines. **D)** Same as C for the Bjarnarflag area.

Figure 2: Overview of data collected at Krafla and Bjarnarflag areas since 1993. **A)** Number of leveling sites surveyed each year. **B)** Number of GPS sites surveyed each year. **C)** InSAR time series coverage for each track. **D)** Water and steam extraction and injection at Krafla and Bjarnarflag power plants.

Figure 3: Overview of ground deformation measurements between 1993 and 2003. **A)** Vertical velocities (arrows with yellow head and black lines) derived from leveling measurements between 1995 and 2005 (referenced to the yellow star location). Extraction (red) and injection (blue) rates for boreholes between summer 1993 and summer 2004 are shown by the histogram bars and their associated colored hexagons. Background shows shaded topography, Krafla caldera (comb line), 1975-1984 lavas (gray area), and main road (black line). **B)** ERS T9 InSAR time series. Left: Average LOS velocity for each PS. Profiles (colored dotted lines), sampling area for time series (black circle), and satellite look direction (arrow) are indicated. Up: profiles across the Krafla geothermal area (blue), the Bjarnarflag area (red), and between (green). Right: time series of average LOS displacement at Krafla (blue) and Bjarnarflag (red) sampling areas. **C)** ERS T52 InSAR time series. **D)** ERS T281 InSAR time series.

Figure 4: Overview of ground deformations measurements between 2004 and 2010. Data presented in the same way as in Fig. 3, with addition of GPS vertical velocities (green arrows) and horizontal velocities (purple arrows) shown in **A)**.

Figure 5: Overview of ground deformations measurements between 2009 and 2014. Data presented in the same way as in Fig. 4.

Figure 6: Overview of ground deformations measurements between 2012 and 2015. Data presented in the same way as in Fig. 4.

Figure 7: (Upper) Areas of high deformation gradient derived from stacking all InSAR time series. (Lower) Areas of high deformation gradient derived from stacking InSAR time series for each time interval. Results in areas of high slope are masked out. See Section 2.5 for explanation. Background shows shaded topography, Krafla caldera (comb lines), and main road (black line). Placenames of interest are indicated (Lh: Leirhnjúkur, Lb: Leirbotnar, H: Hvíthólar, B: Bjarnarflag). Boreholes which were used for production between 1993 and 2015 are shown with blue hexagons. Path of boreholes which are not vertical are shown with blue lines.

Figure 8: Time interval 2009-2014: GPS horizontal (first row), GPS vertical (second row), resampled TSX T49 (third row), resampled TSX T56 (forth row). Data (first column), model (second column), and residuals (third column). Model includes point pressure sources (white circles), plate spreading (dashed line), and a narrow elongated sill (striped line). The sources (listed in Table 2) are shown color coded in the first row middle column, with the same colors used in Figs. 9 and 10: narrow elongated sill (orange), *Bjarnarflag* (light blue), *Leirbotnar* (green), $Deep_{inflation}$ (red), and $Deep_{deflation}$ and *Leirhnjkur* (dark blue). Note that the $Deep_{deflation}$ source is directly below *Leirhnjukur* and therefore both appear as a single point. Background shows caldera rim (thin line), 1975-1984 lava field (gray area), and main road (black line).

Figure 9: Inversion results for tectonic and magmatic sources for different time intervals (see Section 3.2.1 for explanations). **A)** Closing rate of the sill. **B)** Volume change of the $Deep_{inflation}$ source (red) and the $Deep_{deflation}$ source (blue). **C)** Volume change of the shallow deflation source beneath Leirhnjúkur (red). Error bars show time interval (X-axis) and 95% confidence interval (Y-axis). Parameters values are given in Table 3.

Figure 10: Inversion results for geothermal sources for different time intervals (see Section 3.2.1 for explanations). **A)** Volume change of the deflation source beneath Leirbotnar (line) and water and steam net extraction rate at Krafla power plant (bars). Error bars show time interval (X-axis) and 95% confidence interval (Y-axis, only for shallow pressure sources). Parameters values are given in Table 3. Net extraction rate derived from the same data as shown in Fig. 2D. **B)** Volume change of the deflation source beneath Bjarnarflag (line) and water and steam net extraction rate at Bjarnarflag power plant (bars). **C)** Comparison of the cumulative volume change of the sources beneath Krafla (dark green) and Bjarnarflag (dark blue) with water and steam cumulative net mass extraction at Krafla (light green) and Bjarnarflag (light blue) power plants. For each year, the cumulative volume change is calculated by adding the estimated yearly volume change (as shown in A and B) over the year. In case of overlapping time periods studied, the average of the estimated yearly volume change is used.

24

Table 1: Dataset for each time intervals. For 2004-2010 and 2009-2014 time intervals, only GPS sites with at least 3 years between their first and last measurements during these time intervals were considered. For 2012-2015, only GPS sites with at least 2 years between their first and last measurements were considered. Each dataset consists of the average velocities derived over the time interval (InSAR and GPS), or the enclosing time interval (leveling).

	1993-1995	1995-2000	2000-2003	2004-2010	2009-2014	2012-2015
GPS	-	-	-	2004-2010	2009-2014	2012-2015
leveling	-	1995-2000	2000-2005	2005-2010	-	-
InSAR	ERS T9	ERS T9, T52, T281	ERS T9, T52	Envi T230, T281	TSX T49, T56	TSX T147, RS2

Table 2: Best fitting model parameters of the regional deformation signal 2009-2014. Parameters indicated with * were inverted for (see text). Full description of the spreading segment models and their parameters are given in Drouin et al. (2017).

Mogi sources	Lon.[°E]	Lat.[°N]	Depth[km]	ΔVolume[m^3/yr]			
Deep$_{inflation}$	-16.730	65.832	21.5	6.0x10^6*			
Deep$_{deflation}$	-16.7975	65.7150	21.5	-9.0x10^6*			
Leirhnjukur	-16.7975	65.7150	2.5	-0.09x10^6			
Leirbotnar	-16.76718	65.70751	1.5	-0.04x10^6			
Bjarnarflag	-16.86294	65.63937	1.5	-0.04x10^6			
Spreading segments	**Lon.[°E]**	**Lat.[°N]**	**Lon.[°E]**	**Lat.[°N]**	**Locking depth[km]**		
HFF4	-16.726	65.884	-17.349	66.047	6.3		
GOR3	-16.726	65.884	-16.580	66.242	4.5		
Krafla	-16.798	65.70	-16.726	65.884	6		
Fremirinamar	-16.592	65.37	-16.798	65.70	8		
Okada sill	**Lon.[°E]**	**Lat.[°N]**	**Lon.[°E]**	**Lat.[°N]**	**Depth[km]**	**Width[km]**	**Closing rate[mm/yr]**
Fissure swarm	-16.893	65.544	-16.549	66.190	3.3*	0.6*	-28*

Table 3: Best fitting model parameters for each time intervals. Sources details are given in Table 2. The search range used in inversion for each parameters is also indicated.

Sources	Parameters	Search range	1993-1995	1995-2000	2000-2003	2004-2010	2009-2014	2012-2015
Deep$_{inflation}$	Volume change [x10^6 m^3/yr]	0 to 40	35^{+4}_{-13}	35^{+5}_{-14}	33^{+5}_{-14}	14^{+9}_{-7}	6^{+6}_{-4}	1^{+5}_{-1}
Deep$_{deflation}$	Volume change [x10^6 m^3/yr]	0 to -40	-29^{+21}_{-7}	-27^{+21}_{-10}	-30^{+22}_{-8}	-22^{+10}_{-11}	-17^{+10}_{-6}	-21^{+8}_{-4}
Fissure swarm	Opening [mm/yr]	0 to -100	-57^{+14}_{-19}	-58^{+15}_{-13}	-52^{+14}_{-15}	-45^{+14}_{-16}	-41^{+10}_{-11}	-33^{+12}_{-28}
Leirhnjukur	Volume change [x10^4 m^3/yr]	0 to -20	$-15.9^{+7.6}_{-4.1}$	$-2.9^{+2.5}_{-8.8}$	$-2.4^{+2.0}_{-8.5}$	$-0.6^{+0.4}_{-5.2}$	$-0.7^{+0.4}_{-4.9}$	$-0.7^{+0.4}_{-2.9}$
Leirbotnar	Volume change [x10^4 m^3/yr]	0 to -15	$-9.2^{+2.8}_{-3.6}$	$-10.4^{+4.1}_{-1.7}$	$-9.2^{+4.1}_{-2.4}$	$-2.6^{+2.0}_{-2.8}$	$-4.2^{+2.9}_{-2.9}$	$-5.8^{+3.6}_{-2.8}$
Bjarnarflag	Volume change [x10^4 m^3/yr]	0 to -15	$-0.8^{0.7+}_{-2.8}$	$-1.7^{+1.2}_{-2.8}$	$-1.7^{+1.3}_{-2.8}$	$-5.6^{+2.5}_{-2.8}$	$-4.2^{+2.2}_{-3.5}$	$-10.3^{+3.2}_{-3.2}$

Ali, S., Akerley, J., Baluyut, E., Cardiff, M., Davatzes, N., Feigl, K., Foxall, W., Fratta, D., Mellors, R., Spielman, P., Wang, H., Zemach, E., 2016. Time-series analysis of surface deformation at Brady Hot Springs geothermal field (Nevada) using interferometric synthetic aperture radar. Geothermics 61, 114–120.

Ali, S. T., Feigl, K. L., Carr, B. B., Masterlark, T., Sigmundsson, F., 2014. Geodetic measurements and numerical models of rifting in Northern Iceland for 1993–2008. Geophysical Journal International.

Auriac, A., Sigmundsson, F., Hooper, A., Spaans, K. H., Björnsson, H., Pálsson, F., Pinel, V., Feigl, K. L., 2014. InSAR observations and models of crustal deformation due to a glacial surge in Iceland. Geophysical Journal International 198, 1329–1341.

Axelsson, G., Arnaldsson, A., Berthet, J.-C. C., Bromley, C. J., Gudnason, E. A., Hreinsdóttir, S., Karlsdóttir, R., Magnússon, I. T., Michalczewska, K. L., Sigmundsson, F., Sigurdsson, O., 2015. Renewability Assessment of the Reykjanes Geothermal System, SW-Iceland. In: Proceedings World Geothermal Congress. Melbourne, Australia, 19-25 April 2015.

Bromley, C., Brockbank, K., Glynn-Morris, T., Rosenberg, M., Pender, M., O'Sullivan, M., Currie, S., 2013. Geothermal subsidence study at Wairakei-Tauhara, New Zealand. Proceedings of the Institution of Civil Engineers - Geotechnical Engineering 166 (2), 211–223.

Buck, W. R., Einarsson, P., Brandsdóttir, B., 2006. Tectonic stress and magma chamber size as controls on dike propagation: Constraints from the 1975–1984 Krafla rifting episode. Journal of Geophysical Research: Solid Earth 111.

Budzińska, K., 2014. Man made deformation in the Hengill area between 2009-2013. Master's thesis, Faculty of Earth Sciences, University of Iceland.

Chen, Z., 2011. Poroelastic model for induced stresses and deformations in hydrocarbon and geothermal reservoirs. Journal of Petroleum Science and Engineering 80 (1), 41 – 52.

Compton, K., Bennett, R., Hreinsdóttir, S., 2015. Climate driven vertical acceleration of Icelandic crust measured by CGPS geodesy. Geophysical Research Letters 42 (3), 743–750.

de Zeeuw-van Dalfsen, E., Pedersen, R., Sigmundsson, F., Pagli, C., 2004. Satellite radar interferometry 1993–1999 suggests deep accumulation of magma near the crust-mantle boundary at the Krafla volcanic system, Iceland. Geophysical Research Letters 31.

DeMets, C., Gordon, R. G., Argus, D. F., 2010. Geologically current plate motions. Geophysical Journal International 181, 1–80.

Drouin, V., Heki, K., Sigmundsson, F., Hreinsdóttir, F., Ófeigsson, B. G., 2016. Constraints on seasonal load variations and regional rigidity from continuous GPS measurements in Iceland, 1997-2014. Geophysical Journal International.

Drouin, V., Sigmundsson, F., Ófeigsson, B. G., Hreinsdóttir, S., Sturkell, E., Einarsson, P., 2017. Deformation in the northern volcanic zone of iceland 2008-2014: an interplay of tectonic, magmatic, and glacial isostatic deformation. Journal of Geophysical Research: Solid Earth.

Egilson, T., Tryggvason, H., Sveinbjörnsson, B. M., December 2015. Eftirlitsmælingar í Kröflu og Bjarnarflagi árið 2015. Tech. Rep. LV-2015-132, Landsvirkjun.

Einarsson, P., 1991. Umbrotin við Kröflu 1975-89. In: Garðarsson, A., Einarsson, A. (Eds.), Náttúra Mývatns. Hið íslenska náttúrufræðifélag, Reykjavík, Ch. 2, pp. 96–139.

Foulger, G. R., Beutler, G., Bilham, R., Einarsson, P., Fankhauser, S., Gurtner, W., Hugentobler, U., Morgan, W. J., Rothacher, M., Thorbergsson, G., Wild, U., 1993. The Iceland 1986 GPS geodetic survey: tectonic goals and data processing results. Bulletin géodésique 67 (3), 148–172.

Foulger, G. R., Jahn, C.-H., Seeber, G., Einarsson, P., Julian, B. R., Heki, K., 1992. Post-rifting stress relaxation at the divergent plate boundary in Northeast Iceland. Nature 358, 488–490.

Fukushima, Y., Cayol, V., Durand, P., 2005. Finding realistic dike models from interferometric synthetic aperture radar data: The February 2000 eruption at Piton de la Fournaise. Journal of Geophysical Research: Solid Earth 110 (B3).

FUTUREVOLC, 2016. Iceland volcanoes supersite. http://futurevolc.hi.is/iceland-volcanoes-supersite, accessed: 2016-05-11.

Gerke, K., 1974. Crustal movements in the Myvatn and in the Thingvallavatn area, both horizontal and vertical. In: Kristjansson, L. (Ed.), Geodynamics of Iceland and the North Atlantic Area. D. Reidel publishing company, Dordrecht, pp. 263–275.

Grandin, R., Socquet, A., Doin, M.-P., Jacques, E., de Chabalier, J.-B., King, G. C. P., 2010. Transient rift opening in response to multiple dike injections in the Manda Hararo rift (Afar, Ethiopia) imaged by time-dependent elastic inversion of interferometric synthetic aperture radar data. Journal of Geophysical Research: Solid Earth 115 (B9).

Grapenthin, R., Sigmundsson, F., Geirsson, H., Árnadóttir, T., Pinel, V., 2006. Icelandic rhythmics: Annual modulation of land elevation and plate spreading by snow load. Geophysical Research Letters 33 (24).

Hamling, I. J., Wright, T. J., Calais, E., Lewi, E., Fukahata, Y., apr 2014. InSAR observations of post-rifting deformation around the Dabbahu rift segment, Afar, Ethiopia. Geophysical Journal International 197, 33–49.

Heki, K., Foulger, G. R., Julian, B. R., Jahn, C., 1993. Plate dynamics near divergent boundaries: geophysical implications of postrifting crustal deformation in NE Iceland. Journal of Geophysical Research 98, 14279–14297.

Herring, T., McClusky, S., 2009. GAMIT/GLOBK MATLAB TOOLS. www-gpsg.mit.edu/ tah/GGMatlab/.

Hjartardóttir, A. R., Einarsson, P., Bramham, E., Wright, T. J., 2012. The Krafla fissure swarm, Iceland, and its formation by rifting events. Bulletin of Volcanology 74, 2139–2153.

Hjartardóttir, A. R., Einarsson, P., Magnúsdóttir, S., Björnsdóttir, T., Brandsdóttir, B., 2015. Fracture systems of the Northern Volcanic Rift Zone, Iceland: an onshore part of the Mid-Atlantic plate boundary. Geological Society, London, Special Publications 420.

Hofton, M. A., Foulger, G. R., 1996. Postrifting anelastic deformation around the spreading plate boundary, north Iceland: 1. Modeling of the 1987–1992 deformation field using a viscoelastic Earth structure. Journal of Geophysical Research: Solid Earth 101 (B11), 25403–25421.

Hole, J., Bromley, C., Stevens, N., Wadge, G., 2007. Subsidence in the geothermal fields of the Taupo Volcanic Zone, New Zealand from 1996 to 2005 measured by InSAR. Journal of Volcanology and Geothermal Research 166 (3–4), 125–146.

Hooper, A., 2008. A multi-temporal InSAR method incorporating both persistent scatterer and small baseline approaches. Geophysical Research Letters 35 (16).

Im, K., Elsworth, D., Guglielmi, Y., Mattioli, G. S., 2017. Geodetic imaging of thermal deformation in geothermal reservoirs - production, depletion and fault reactivation. Journal of Volcanology and Geothermal Research 338, 79 – 91.

Islam, M. T., Sturkell, E., LaFemina, P., Geirsson, H., Sigmundsson, F., Ólafsson, H., 2016. Continuous subsidence in the Thingvellir rift graben, Iceland: Geodetic observations since 1967 compared to rheological models of plate spreading. Journal of Geophysical Research: Solid Earth 121 (1), 321–338.

Jahn, C.-H., Seeber, G., Foulger, G., Björnsson, A., 1990. A GPS Survey in the North-East Volcanic Zone of Iceland 1987 First Results. In: Vyskocil, P., Reigber, C., Cross, P. (Eds.), Global and Regional Geodynamics. Vol. 101 of International Association of Geodesy Symposia. Springer New York, pp. 173–181.

Juncu, D., Árnadóttir, T., Hooper, A., Gunnarsson, G., 2017. Anthropogenic and natural ground deformation in the Hengill geothermal area, Iceland. Journal of Geophysical Research: Solid Earth 122 (1), 692–709.

Keiding, M., Árnadóttir, T., Jónsson, S., Decriem, J., Hooper, A., 2010. Plate boundary deformation and man-made subsidence around geothermal fields on the Reykjanes Peninsula, Iceland. Journal of Volcanology and Geothermal Research 194 (4), 139 – 149.
URL http://www.sciencedirect.com/science/article/pii/S0377027310001290

Lundgren, P., Poland, M., Miklius, A., Orr, T., Yun, S.-H., Fielding, E., Liu, Z., Tanaka, A., Szeliga, W., Hensley, S., Owen, S., 2013. Evolution of dike opening during the March 2011 Kamoamoa fissure eruption, Kilauea Volcano, Hawai'i. Journal of Geophysical Research: Solid Earth 118 (3), 897–914.

Masterlark, T., Lu, Z., 2004. Transient volcano deformation sources imaged with interferometric synthetic aperture radar: Application to Seguam Island, Alaska. Journal of Geophysical Research: Solid Earth 109 (B1).

Metzger, S., Jónsson, S., 2014. Plate boundary deformation in North Iceland during 1992–2009 revealed by InSAR time-series analysis and GPS. Tectonophysics 634, 127–138.

Metzger, S., Jónsson, S., Danielsen, G., Hreinsdóttir, S., Jouanne, F., Giardini, D., Villemin, T., 2012. Present kinematics of the Tjornes Fracture Zone, North Iceland, from campaign and continuous GPS measurements. Geophysical Journal International.

Mogi, K., 1958. Relations between the Eruptions of Various Volcanoes and the Deformations of the Ground Surfaces around them. Bulletin of the Earthquake Research Institute 36, 99–134.

Niemczyk, O., 1943. Splaten auf Island. Konrad Wittwer Verlag, Stuttgart.

Nooner, S. L., Bennati, L., Calais, E., Buck, W. R., Hamling, I. J., Wright, T. J., Lewi, E., 2009. Post-rifting relaxation in the Afar region, Ethiopia. Geophysical Research Letters 36 (21).

Okada, Y., 1992. Internal deformation due to shear and tensile faults in a half-space. Bulletin of the Seismological Society of America 82 (2), 1018–1040.
URL http://www.bssaonline.org/content/82/2/1018.abstract

Pedersen, R., Sigmundsson, F., Masterlark, T., 2009. Rheologic controls on inter-rifting deformation of the Northern Volcanic Zone, Iceland. Earth and Planetary Science Letters 281, 14–26.
URL http://www.sciencedirect.com/science/article/pii/S0012821X09000806

Pritchard, M. E., Simons, M., 2006. An aseismic slip pulse in northern Chile and along-strike variations in seismogenic behavior. Journal of Geophysical Research: Solid Earth 111 (B8).

Rinaldi, A., Todesco, M., Bonafede, M., 2010. Hydrothermal instability and ground displacement at the Campi Flegrei caldera. Physics of the Earth and Planetary Interiors 178 (3–4), 155 – 161.

Sigmundsson, F., Vadon, H., Massonnet, D., 1997. Readjustment of the Krafla spreading segment to crustal rifting measured by satellite radar interferometry. Geophysical Research Letters 24 (15), 1843–1846.

Smittarello, D., Grandin, R., De Chabalier, J.-B., Doubre, C., Deprez, A., Masson, F., Socquet, A., Saad, I. A., 2016. Transient deformation in the Asal-Ghoubbet Rift (Djibouti) since the 1978 diking event: Is deformation controlled by magma supply rates? Journal of Geophysical Research: Solid Earth 121 (8), 6030–6052.

Statistics Iceland, 2016. `http://statice.is/`, accessed: 2016-04-28.

Sturkell, E., Sigmundsson, F., Geirsson, H., Ólafsson, H., Theodórsson, T., 2008. Multiple volcano deformation sources in a post-rifting period: 1989–2005 behaviour of Krafla, Iceland constrained by levelling, tilt and GPS observations. Journal of Volcanology and Geothermal Research 177 (2), 405–417.
URL `http://www.sciencedirect.com/science/article/pii/S0377027308003429`

Sæmundsson, K., 1974. Evolution of the Axial Rifting Zone in Northern Iceland and the Tjörnes Fracture Zone. Geological Society of America Bulletin 85 (4), 495–504.
URL `http://gsabulletin.gsapubs.org/content/85/4/495.abstract`

Sæmundsson, K., 1991. Jarðfræði Kröflukerfisins. In: Garðarsson, A., Einarsson, A. (Eds.), Náttúra Mývatns. Hið íslenska náttúrufræðifélag, Reykjavík, Ch. 1, pp. 24–95.

Theodórsson, T., Búi, J., April 2011. Krafla, Mývatn, fínhæðarmælingar 2010. Tech. Rep. LV-2011/048, Landsvirkjun.

Thoroddsen, T. e., 1907–1915. Skýrslur um Mývatnselda 1724-1729. Safn til sögu Íslands 4, 385–411.

Tryggvason, E., 1984. Widening of the Krafla fissure swarm during the 1975–1981 volcano-tectonic episode. Bulletin Volcanologique 47 (1), 47–69.

Vasco, D. W., Rutqvist, J., Ferretti, A., Rucci, A., Bellotti, F., Dobson, P., Oldenburg, C., Garcia, J., Walters, M., Hartline, C., 2013. Monitoring deformation at the Geysers Geothermal Field, California using C-band and X-band interferometric synthetic aperture radar. Geophysical Research Letters 40 (11), 2567–2572.

Wendt, K., Möller, D., Ritter, B., 1985. Geodetic measurements of surface deformations during the present rifting episode in NE Iceland. Journal of Geophysical Research: Solid Earth 90 (B12), 10163–10172.

Wessel, P., Smith, W. H. F., 1998. New, improved version of generic mapping tools released. Eos, Transactions AGU 79, 579–579.

Árnadóttir, T., Lund, B., Jiang, W., Geirsson, H., Björnsson, H., Einarsson, P., 2009. Glacial rebound and plate spreading: results from the first countrywide GPS observations in Iceland. Geophysical Journal International 177, 691–716.

Figures
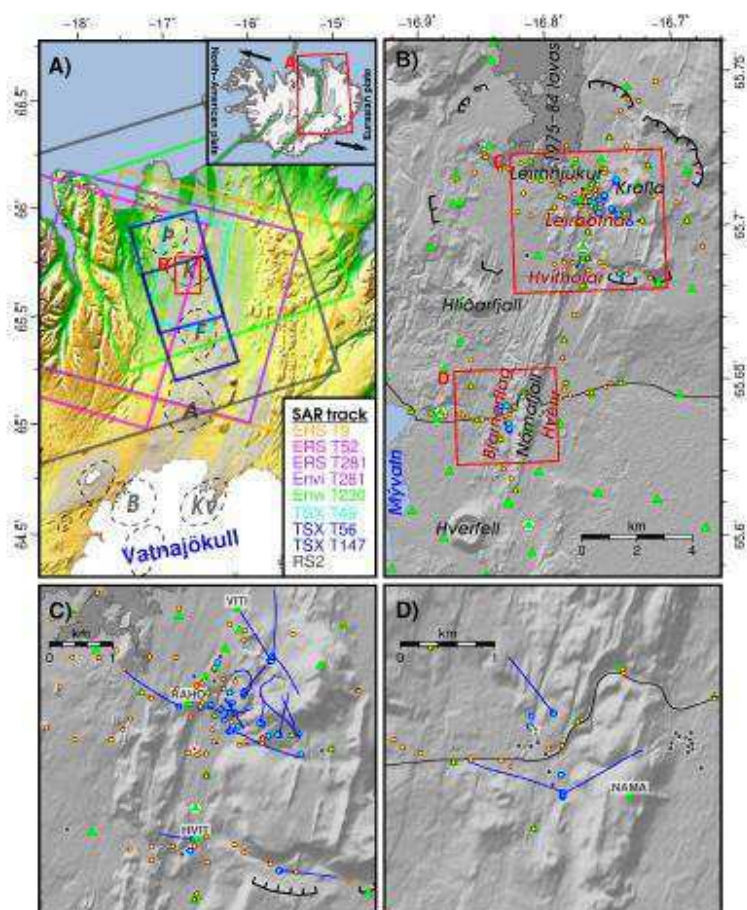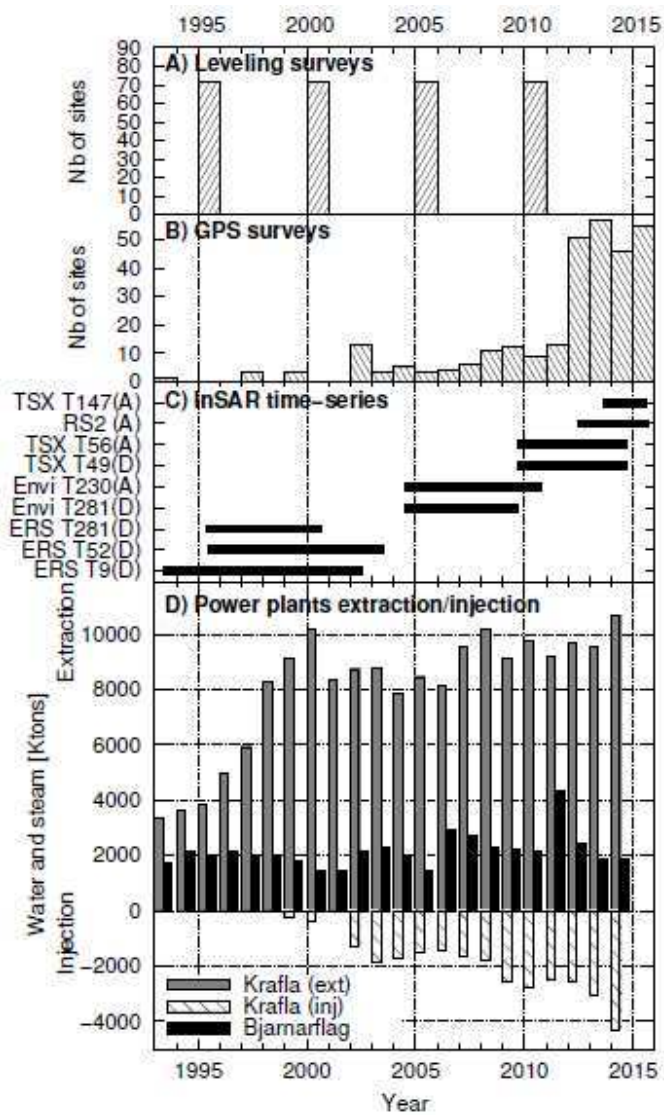
Fig. 1
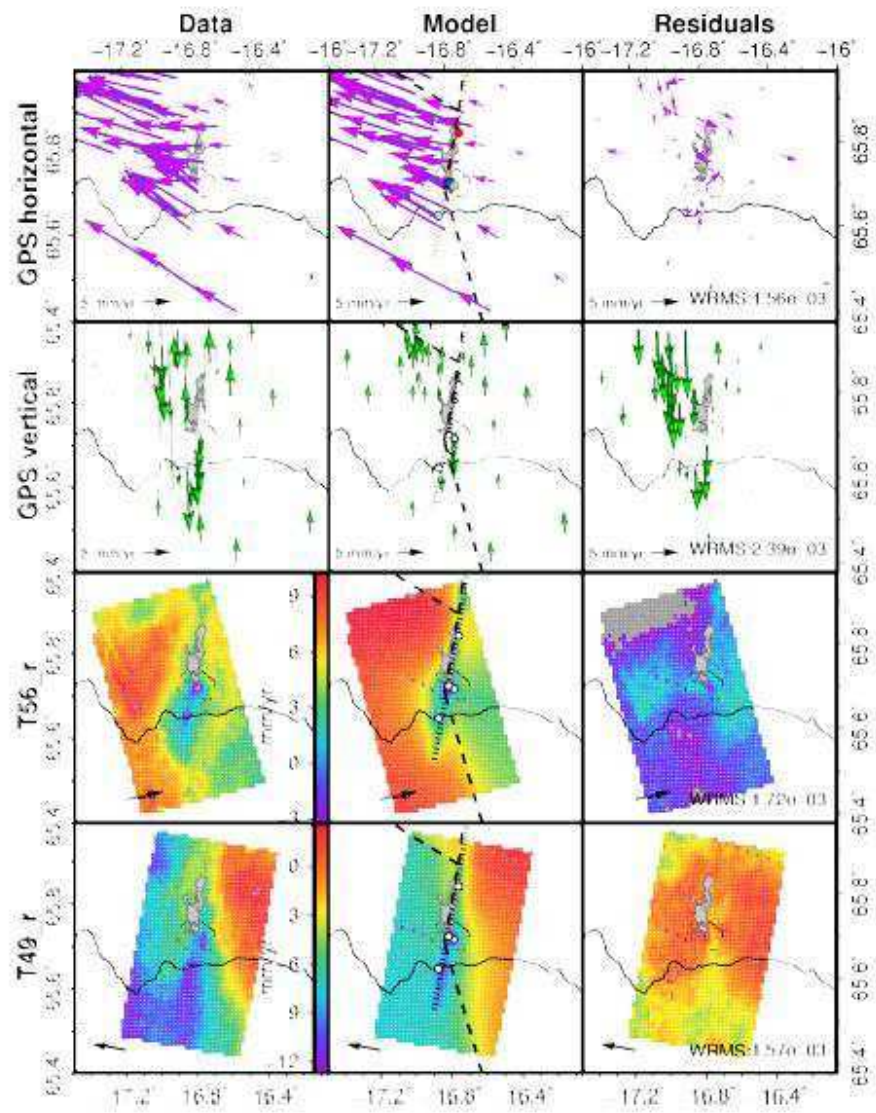
Fig. 2
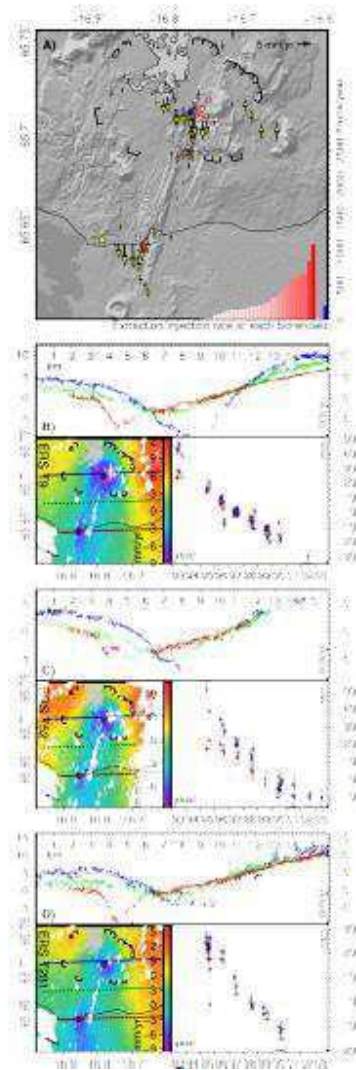
Fig. 3
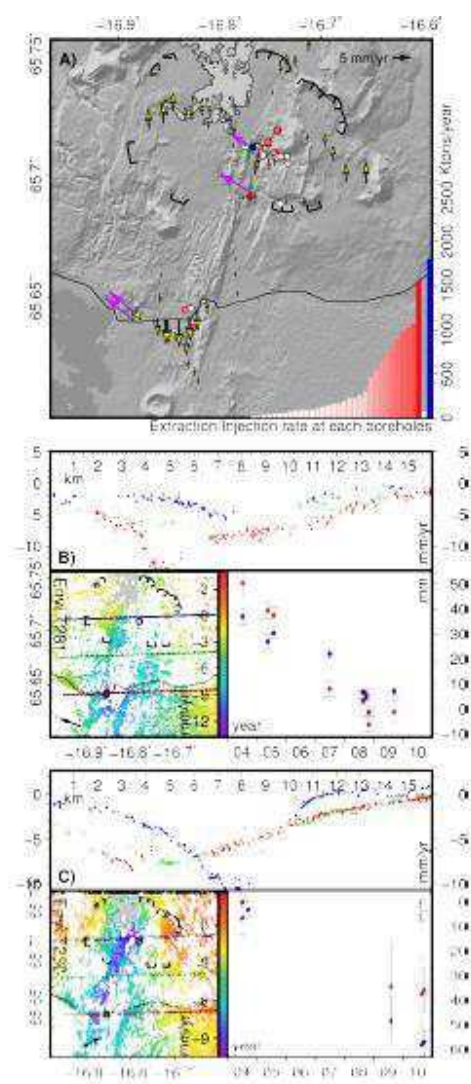
Fig. 4
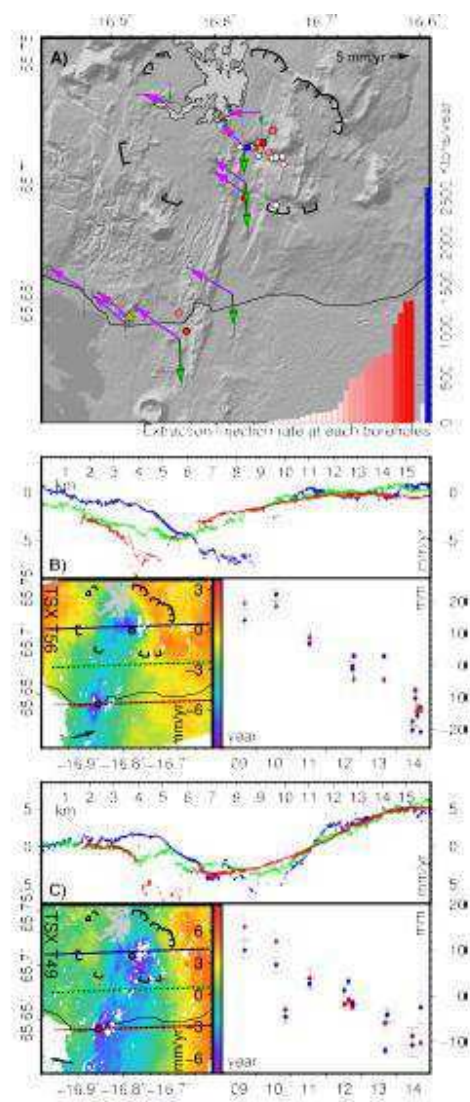
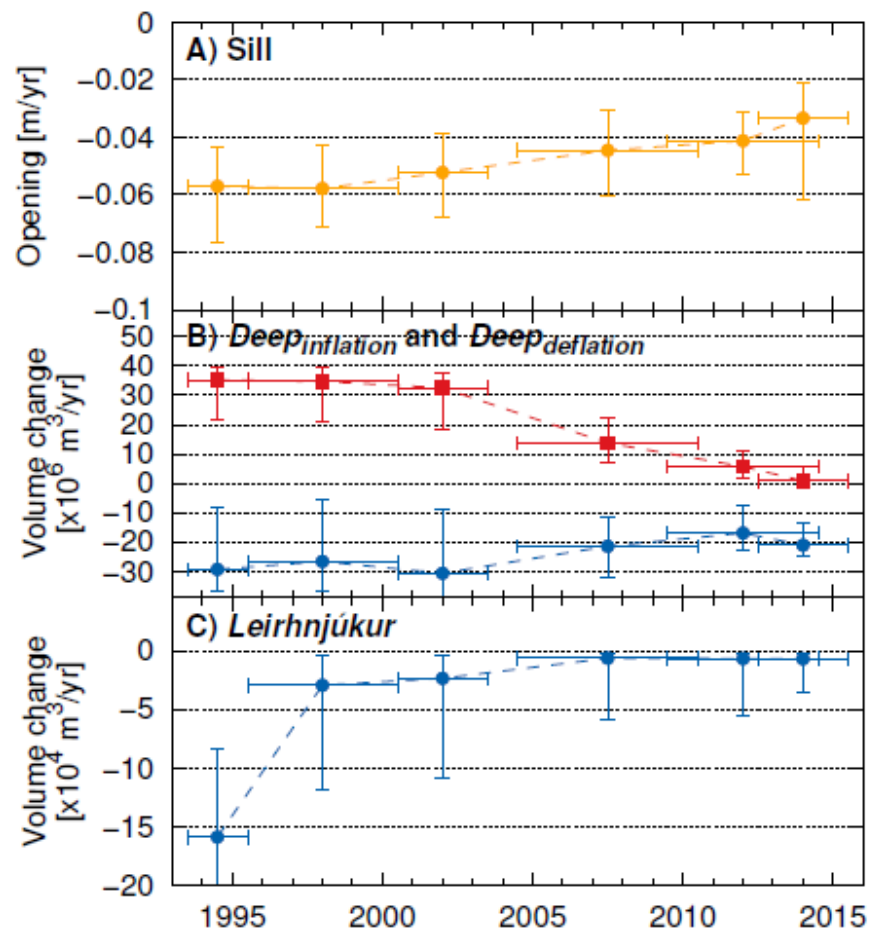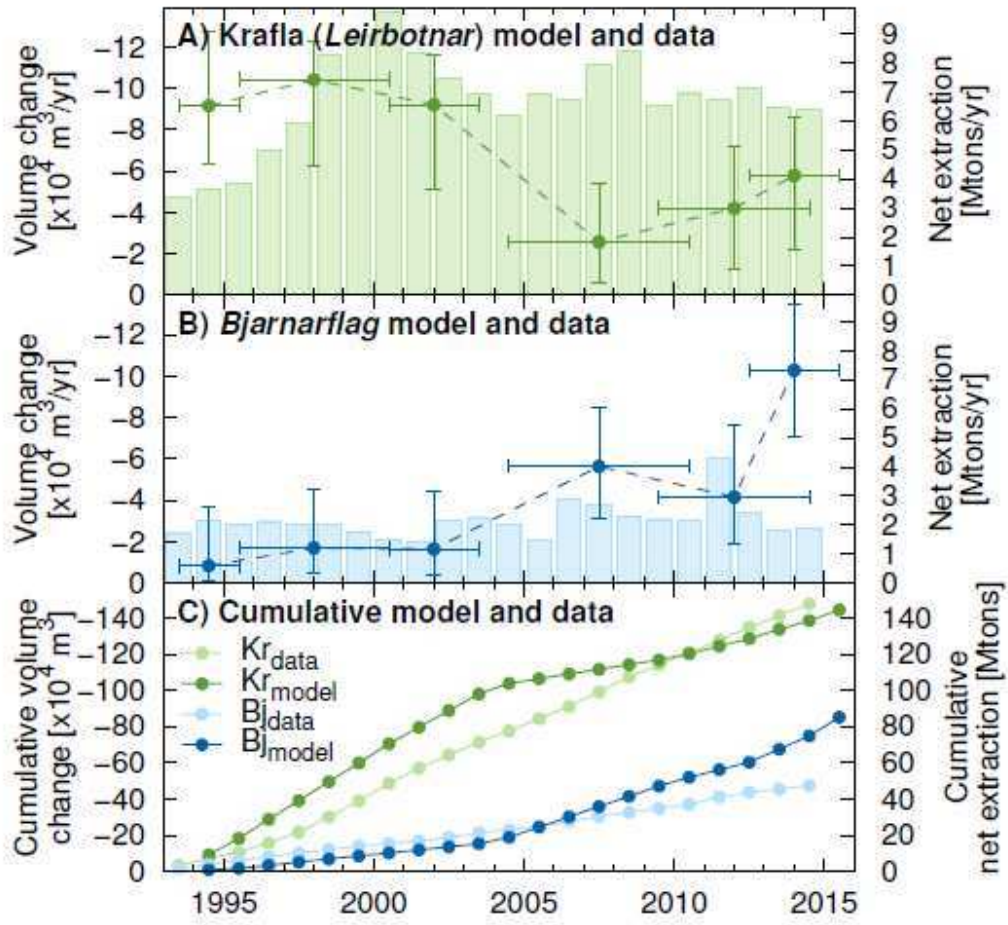Fig. 5
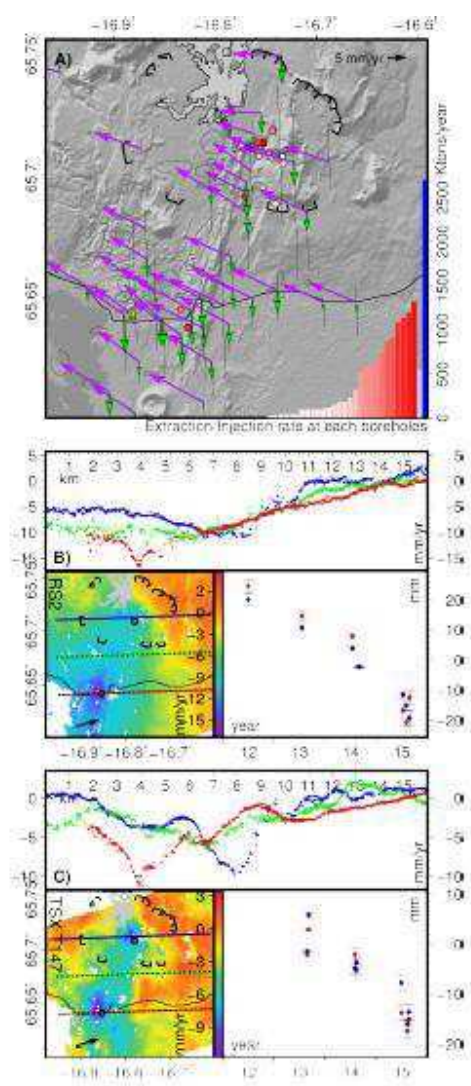
Fig. 6
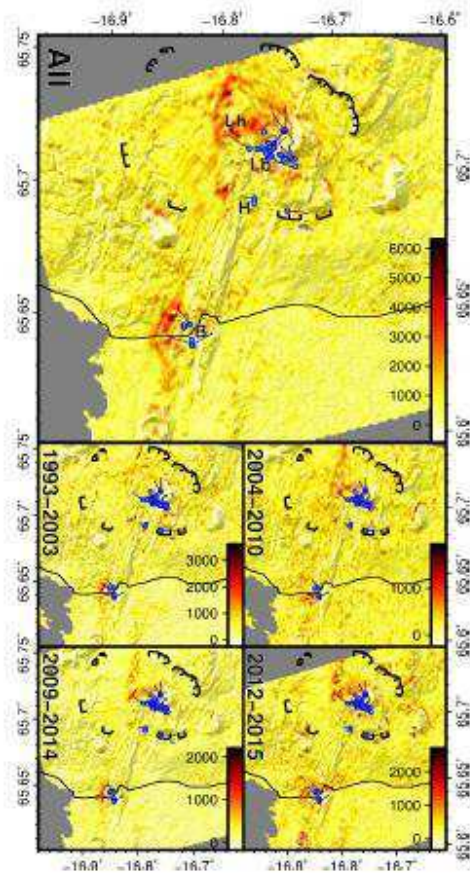
Fig. 7

Fig. 8

Fig. 9

Fig. 10

Highlights

- Local subsidence of about 5-8 mm/yr is observed at geothermal areas
- A pressure source at each utilized borehole can reproduce well the deformation field
- Deformation could possibly relate exclusively to rock cooling down in the reservoir
- Exponential decay of pressure in a shallow magma chamber beneath Krafla is observed